ACS OMEGA

Open Access

http://pubs.acs.org/journal/acsodf

Article

Experimental and Theoretical Approaches to Monitor the Behavior of Bovine Liver Catalase in Interaction with a Binuclear Bismuth Complex

Zahral Alimoradi, Fereshteh Shiri,* Somaye Shahraki, Zohreh Razmara, and Mostafa Heidari-Majd

Cite This: *ACS Omega* 2024, 9, 27071−27084

Read Online

ACCESS | Metrics & More | Article Recommendations | Supporting Information

ABSTRACT: Here, the antioxidant potency of a binuclear Bi(III) complex {$[Bi_2(\mu\text{-ox})(dipic)_2(H_2O)_2(taa)_2].H_2O$, where ox^{2-} = oxalato, $dipic^{2-}$ = pyridine 2,6-dicarboxylato, and taa = thiourea} was evaluated using the •DPPH assay. It was demonstrated that the Bi complex exhibited a high ability to inhibit DPPH free radicals. The binding mechanism of the complex with bovine liver catalase (BLC) was also investigated, revealing structural and activity changes in the enzyme in the presence of the complex. The catalase activity in the decomposition of hydrogen peroxide increased in the presence of the Bi complex, reaching 39.8% higher than its initial activity at a concentration of 7.77×10^{-6} M. The complex exhibited a relatively high affinity for BLC, with K_b values of 3.98, 0.13, and 0.09×10^5 M^{-1} at 303, 310, and 317 K, respectively. The mechanisms involved in the interaction were hydrogen bonding and van der Waals interactions, as validated through molecular docking simulations. Synchronous fluorescence showed that tryptophan was more affected by enzyme−complex interactions than tyrosine. In addition, a cell viability test using the MTT method revealed that at its highest concentration, the Bi complex caused a decrease in the number of cells below 50% compared to the control, while cisplatin showed negative effects at all concentrations. These findings suggest that the Bi complex has the potential to be developed as a promising candidate for BLC-related therapeutic target therapy.

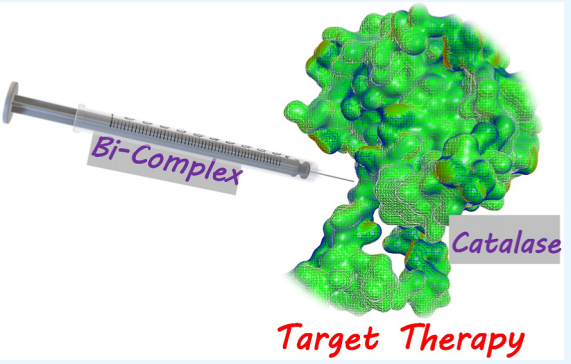

INTRODUCTION

Bismuth is a post-transition metal with low toxicity that can be directly or indirectly related to human life.[1] Various compounds of bismuth have been investigated in pigments, electronic applications, as well as pharmaceuticals.[1−3] Bismuth drugs are often used to treat ulcers caused by *Helicobacter pylori* and some gastrointestinal diseases. Medicines containing bismuth together with antibiotics have synergistic activity and are suitable options to overcome bacterial resistance. Bismuth compounds are often inexpensive, and various studies have confirmed their diverse biological effects, such as antitumor, antifungal, and antiviral. However, compounds containing bismuth have limited bioavailability in physiological environments. Therefore, there have been repeated attempts to synthesize bismuth compounds and explore new approaches to overcome this challenge.[4] Bismuth commonly exhibits a +3 valence state and demonstrates significant chelation potential with multidentate ligands containing nitrogen and oxygen atoms during coordination. This propensity arises from the availability of its three 6p electrons in the topmost layer, which are poised for bond formation.[5]

When exploring the biological characteristics of recombinant medications, it is crucial to examine how these substances interact with essential biological molecules like DNA and enzymes.[6] One of the key enzymes involved in the body's antioxidant defense system and responsible for eliminating reactive oxygen species (ROS) is catalase, primarily synthesized in the liver. Catalase is found in almost all aerobic organisms and in many anaerobic organisms. The function of catalase in the body is to decompose hydrogen peroxide. Insufficient levels of this enzyme in the body can result in the buildup of its substrate, hydrogen peroxide. The accumulation of this reactive oxygen species may contribute to the development of diverse ailments, including cancer and cardiovascular diseases.[7] As previously stated, catalase is primarily synthesized in the liver. The interaction of bovine liver catalase (BLC) with different drugs has been examined in research studies.[8,9] The enzyme consists of four identical subunits, each containing a heme molecule. Each subunit comprises four domains: an α-helical domain, an eight-stranded β-barrel, an N-terminal helix arm, and a connection

Received: January 15, 2024
Revised: May 28, 2024
Accepted: May 30, 2024
Published: June 11, 2024

between the β-barrel and the N-terminal strand arm.[10] The catalytic activity of catalase may be influenced by the presence of different molecules and medications. Reduced enzyme activity can consequently lead to a weakened immune system.[11] Several studies have investigated the impact of drugs on the activity or structure of catalase.[12−14] Notably, catalase has recently been utilized in cancer therapy through pro-oxidant strategies.[15] Catalase plays a significant role in neutralizing H_2O_2. Consequently, any alteration in its activity or expression can disrupt the cellular balance of ROS, which play a dual role in cancer by either activating protumorigenic signals or promoting antitumorigenic signals. Considering the impact of ROS, catalase serves a dual function in cancer, acting both as a tumor suppressor and a protein that supports survival during tumor progression.[16]

Here, we chose the binuclear Bi(III) complex $[Bi_2(\mu\text{-ox})(dipic)_2(H_2O)_2\ (taa)_2].H_2O$ (Figure 1) [CCDC 2079968].[2] This complex was chosen for several reasons: (i) nontoxic metal centers that have the ability to coordinate to various polydentate ligands, (ii) suitable structure of the dipic ligand to form hydrophobic and hydrogen bonds that can be effective in the interaction of the complex with biological molecules such as proteins, and (iii) high solubility of the complex in the aqueous environment, which makes it a candidate for medicine. Several biological investigations have been conducted to assess their capacity to inhibit oxidants like DPPH and their impact on catalase's catalytic efficiency in the decomposition of the toxic hydrogen peroxide, conducted in a comparative manner. Throughout this study, alongside an examination of the catalytic function, structural changes in catalase were also evaluated. Finally, molecular docking studies were employed to investigate the interaction of the complex with catalase and determine the types of forces involved. Results indicate that the Bi complex is a promising candidate for application in BLC-related targeted therapy.

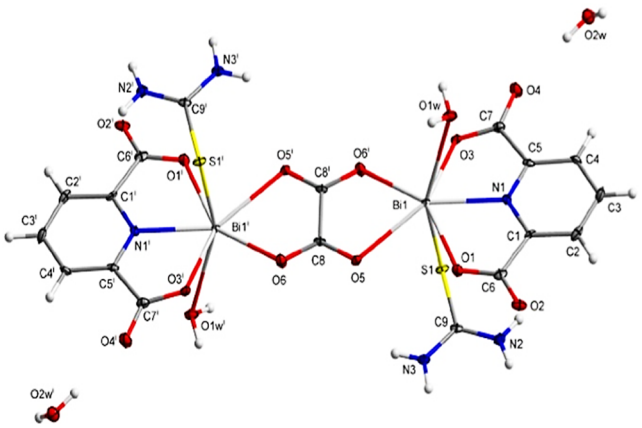

Figure 1. Structure of the Bi complex.

RESULTS AND DISCUSSION

Structure and Hirschfeld Surface Analysis. Figure 2 shows the inter- (Figure 2a) and intramolecular (Figure 2b) hydrogen bonds in the Bi complex. As shown in Figure 2a, the crystal packing of the Bi complex demonstrates strong intermolecular hydrogen bonds between the coordinated and lattice water molecules, which serve as donors, and the oxygen atoms (O1, O2, and O4) of the carboxylate groups, acting as acceptors. There are also other strong hydrogen bonds of types N−H...O (intermolecular) between the oxygen atoms of carboxylate groups and water molecules, which act as an acceptor, with thiourea molecules that act as a donor.

In order to visualize and verify the potential of the Bi complex to form intermolecular hydrogen bonds, Figure 3 shows the 3D d_{norm} surface (3a), 2D fingerprint (3b), and the main interactions (3c) of the Bi complex. The d_{norm} mapping shows strong hydrogen bond of types of O−H...O and O...H−O between coordinated/lattice water molecules and oxygen atoms of carboxylate groups which is in agreement with the crystallographic results. As depicted in the illustration, the red markings indicate the presence of O−H...O and O...H−O hydrogen bonds. These interactions are represented as donor (HO) and acceptor (OH) spikes in the 2D fingerprint plot (Figure 3b). For the title of the complex, the contributions of the OH and HO interactions on the Hirshfeld surface are 25.1 and 16.2%, respectively (Figure 3c). Several interactions with 14.9% contributions are assigned to the dispersive force of H...H. The CH/HC, CO/OC, OO, SH/HS, NH/HN, and CC contacts contribute to 9.3, 5.5, 5.5, 7.1, 1.5, and 3.9%, respectively.

Changes in the Catalytic Activity of Catalase. Examining the impact of various medications, including potential pharmaceuticals, on the enzymatic activity of different enzymes like catalase is crucial.[17,18] The enzymatic performance of BLC can be measured by tracking changes in the enzyme substrate (H_2O_2) concentration. Thus, the alterations in the catalytic efficiency of BLC were assessed when exposed to the Bi complex. The ideal substrate concentration was determined to be 55.5×10^{-3} M. Beyond this concentration, BLC experiences self-inactivation.[19] As seen in Figure 4, in the presence of different concentrations of the Bi complex, the activity of the BLC in the decomposition of hydrogen peroxide has increased so that at a concentration of 4.55×10^{-7} M, the activity of the BLC has increased by 39.2% compared to its initial activity. Metal complexes like [Mn-(phen)2Cl·H2O]Cl.tu, along with medications such as aspirin and the well-known antimalarial drug Artemisinin, have also been noted for their protective properties.[20−22]

Antioxidant Activities. Antioxidant properties of bismuth complex were investigated using the •DPPH free radical. This radical is a stable radical with a delocalized electron. The •DPPH solution exhibits a violet color with a maximum absorption at 517 nm. The reduction of the DPPH radical to hydrazine by the metal complex leads to a color change in the solution from purple to yellow, which can be detected by using UV−vis spectroscopy and colorimetric methods. In this experiment, alcohol (ethanol or methanol) is used to prevent the accumulation of stable DPPH radicals.[23] The graph of free radical inhibition percentage against the Bi complex concentration is shown in Figure 5.

As can be seen, the inhibition of free radicals by the Bi complex at 125 mg/L was 58% after 30 min and increased to 64% after 60 min. Certain functional moieties like hydroxyl groups and aromatic rings possess beneficial characteristics for inhibiting the unpaired electron of free radicals, owing to their electronic properties.[24] The Bi complex's capacity to inhibit •DPPH might be elucidated by the existence of hydroxyl and aromatic rings within the complex. Furthermore, compared to many metal complexes, the Bi complex has better antioxidant capacity.[6,24,25]

https://doi.org/10.1021/acsomega.4c00487
ACS Omega 2024, 9, 27071−27084

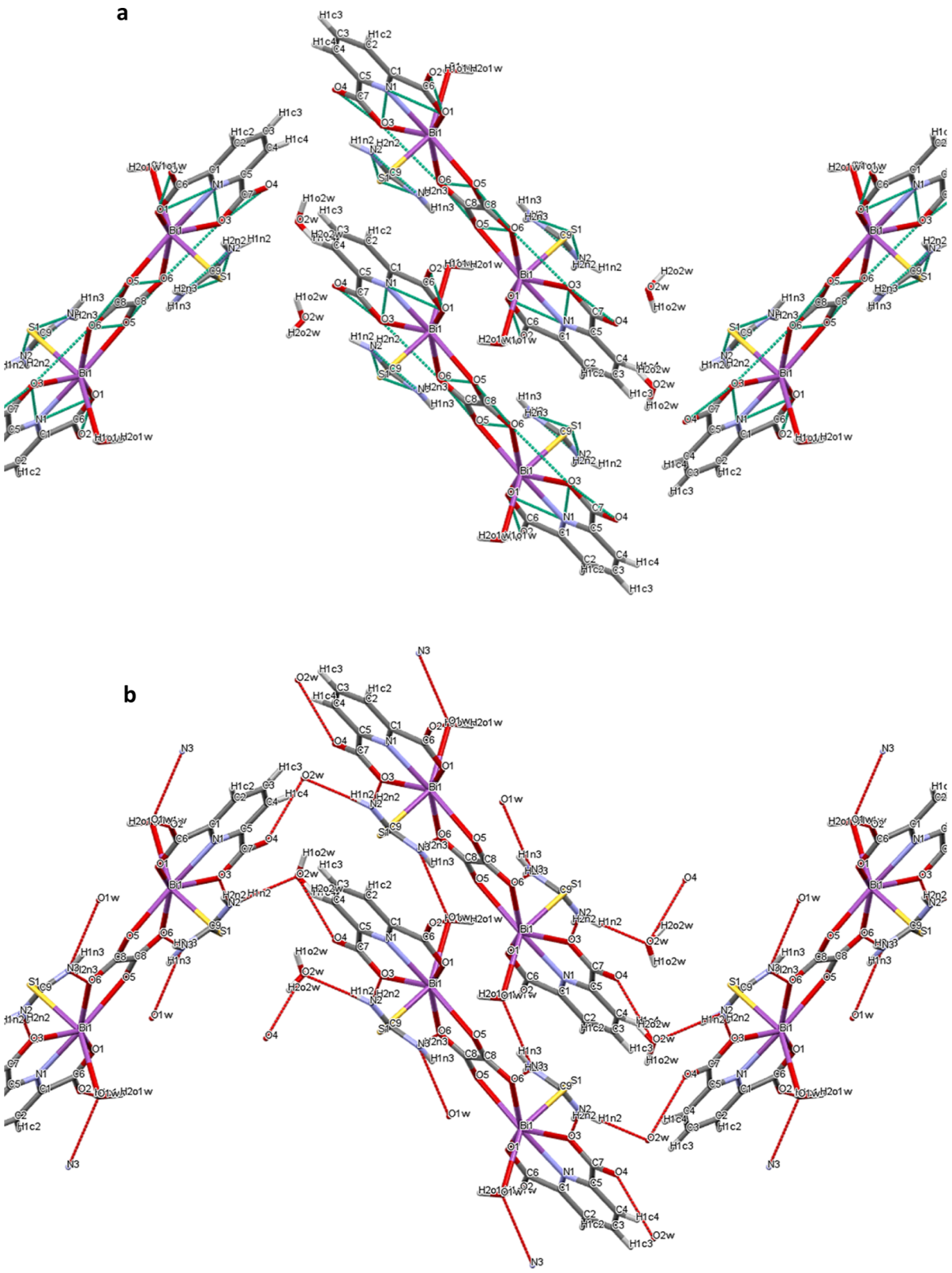

Figure 2. View of (a) intramolecular (green dashed lines) and (b) intermolecular (red dashed lines) hydrogen bonds in the crystal structure of the Bi complex.

BLC-Bi(III) Complex Binding Properties. *Fluorescence Quenching Mechanism and Binding Parameters.* The main source of fluorescence emission in catalase is primarily attributed to two amino acids, tryptophan (Trp) and tyrosine (Tyr). These amino acids are responsive to alterations in the polarity of their surroundings, leading to variations in the fluorescence emission spectrum.

Accordingly, changes in the fluorescence spectrum of BLC were evaluated in the presence of the Bi complex (Figure 6A–C). At the excitation wavelength of 280 nm, the emission

https://doi.org/10.1021/acsomega.4c00487
ACS Omega 2024, 9, 27071−27084

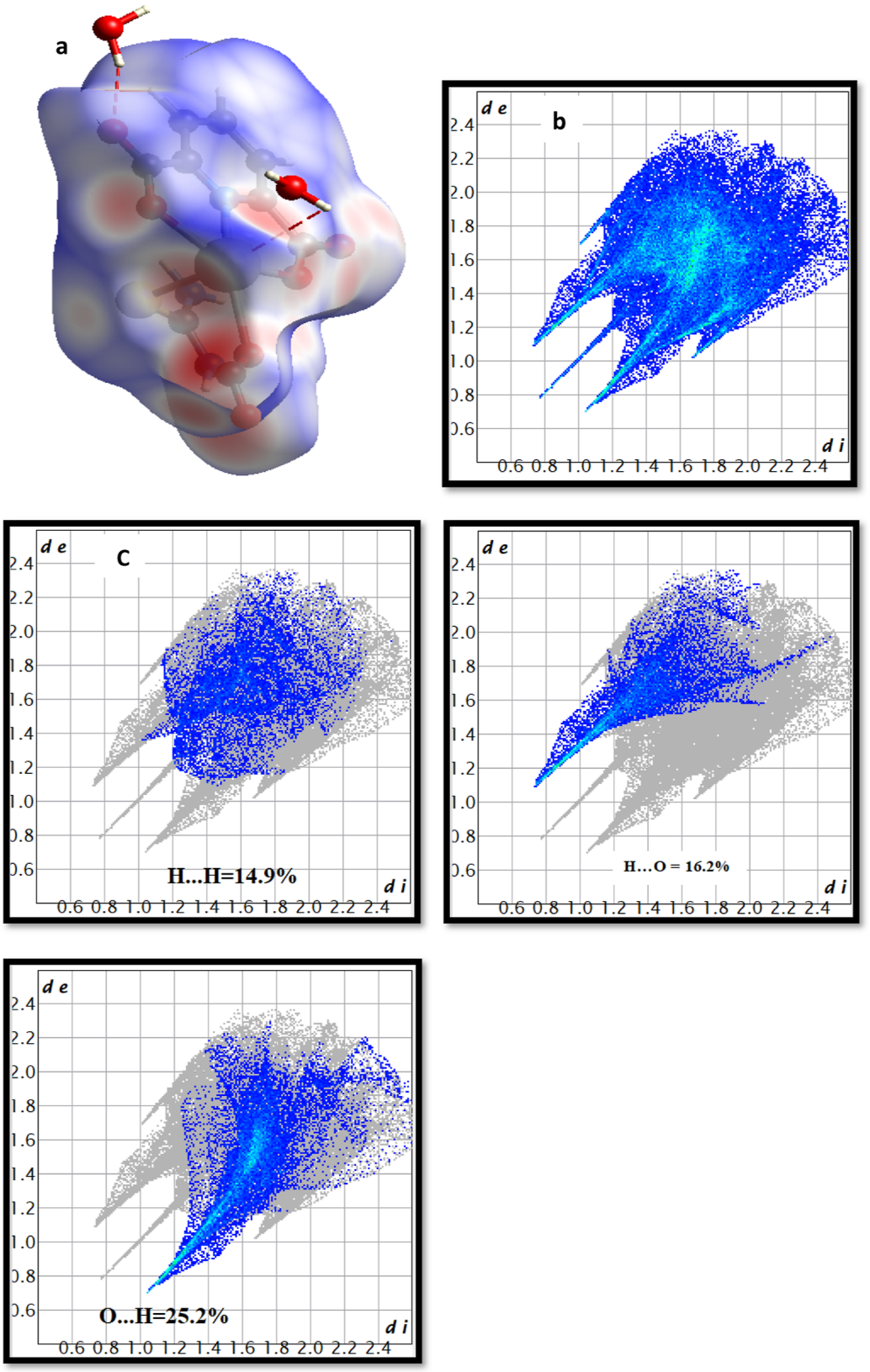

Figure 3. Hirshfeld surface mapped using the d_{norm} function ranging from 1.08 (red) to 1.09 (blue) for the Bi complex (a), the 2D fingerprint (b), and deconvolution illustrating the primary interactions (c).

spectrum of BLC exhibits a wide peak spanning from 300 to 450 nm with λ_{max} = 345 nm. As the concentration of the Bi complex rises, there is a reduction in the intensity of this peak, suggesting that the binding of the Bi complex to the enzyme has the capability to quench the fluorescence emission of the aforementioned amino acids. Within the examined wavelength range, the Bi complex does not exhibit fluorescence emission, thereby ensuring its lack of interference in the subsequent

https://doi.org/10.1021/acsomega.4c00487
ACS Omega 2024, 9, 27071−27084

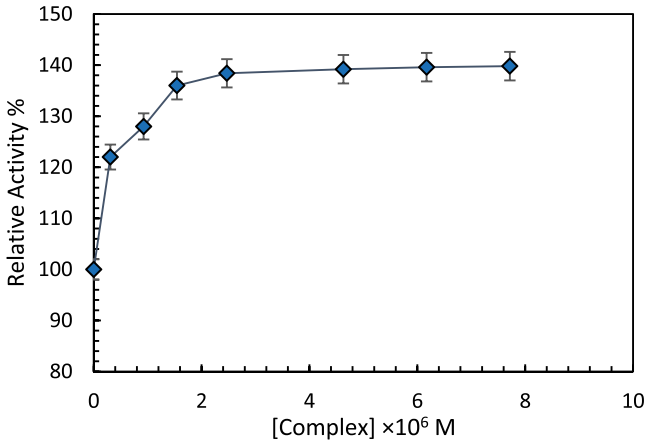

Figure 4. Changes in BLC activity in the presence of the Bi complex. [BLC] = 1.0 × 10^{-8} M, [Bi complex] = (0−8.0 × 10^{-6} M).

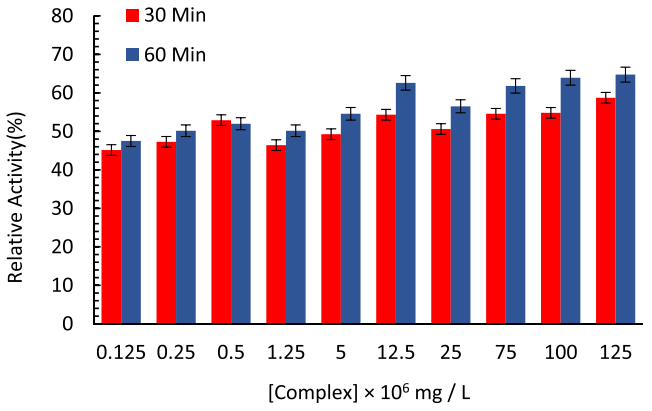

Figure 5. Antioxidant activity of the Bi complex by the DPPH• method.

analysis.[24] Given that the temperature-dependent mechanism governs the quenching of protein fluorescence emission by small molecules, it becomes feasible to anticipate the specific type of mechanism involved.[26] Protein fluorescence quenching can be categorized into three mechanisms: static quenching, initiated by the formation of a ground−state complex between the protein and quenchers; dynamic quenching, arising from collisions between the protein and quenchers; and combined dynamic and static quenching, which results from both collisions and complex formation with the same quencher.[27−30] The constant of maximum dynamic quenching for different quenchers is 2.0 × 10^{10} M^{-1} s^{-1}. Therefore, in the following, fluorescence emission data at three different temperatures of 303, 310, and 317 K were analyzed by the following Stern−Volmer eq 1

$$\frac{F_0}{F} = 1 + k_q\tau_0[Q] = 1 + K_{sv}[Q] \quad (1)$$

where fluorescence intensity of BLC and BLC−Bi complex are F_0 and F, respectively. Quencher (Bi complex) concentration is denoted by $[Q]$ and the Stern−Volmer quenching constant by K_{sv}. By plotting the F_0/F versus Bi complex concentration (Figure 7A), K_{sv} is obtained. The results are presented in Table 1. It is evident that as temperature rises, the K_{sv} values decline. This pattern affirms the presence of a static mechanism in the fluorescence quenching process. Furthermore, the values of k_q were much higher than 2.0 × 10^{10} $M^{-1}.s^{-1}$ (diffusion-limited quenching constant),[31] which again confirms the quenching of fluorescence emission by static mechanism.

One of the important indicators for evaluating the medicinal effects of a drug is its affinity for the receptor. This index aligns with the binding constant (K_b) between the drug and the receptor, where a stronger K_b indicates a higher affinity of the drug to the receptor. The fluorescence quenching results showed that the intrinsic fluorescence of catalase by the Bi complex was carried out through a static quenching mechanism. Therefore, the formation of the nonfluorescent Bi complex-catalase system probably plays the main role in the quenching process.[32]

The binding constant (K_b) and binding stoichiometry of interaction (n) can be obtained with the help of the eq 2[32]

$$\log\frac{F_0 - F}{F} = \log K_b + n\log\left\{[D]_0 - n\frac{[P]_0(F_0 - F)}{F_0}\right\} \quad (2)$$

where $[P]_0$ and $[D]_0$ are the total concentration of protein and drug (ligand), respectively. The curve of $\log\frac{F_0 - F}{F}$ against $\log\left\{[D]_0 - n\frac{[P]_0(F_0 - F)}{F_0}\right\}$ is presented in Figure 7B, where the binding parameters n and K_b are extracted from the slope and Y-intercept of the curves and presented in Table 1. As can be seen, the value of n is almost close to 1 at three temperatures. This indicates that the Bi complex binds with BLC at a molar ratio of 1:1, suggesting a single binding site on BLC. The K_b values were in the order of 10^4 M^{-1}. An inverse relationship is observable between the binding constant (K_b) values and the temperature. As the temperature rises, there is a declining trend in the value of K_b. These results confirm that (i) the relatively strong Bi complex−BLC interactions occurred, (ii) the binding of Bi complex to BLC was an exothermic reaction, and (iii) the affinity of Bi complex toward BLC is comparable to many reported metallic complexes.[6,13,33]

Thermodynamic Analysis. In the interaction between proteins and small molecules, four noncovalent forces—hydrophobic, van der Waals, electrostatic, and hydrogen bonding interactions—play crucial roles. Thermodynamic parameters serve as valuable indicators for predicting the nature of these interactions.[34] To discern the predominant force in the interaction process, two thermodynamic parameters, namely, entropy change ($\Delta S°$) and enthalpy change ($\Delta H°$), are examined for their magnitude and sign. If both $\Delta S°$ and $\Delta H°$ are negative ($\Delta S° < 0$ and $\Delta H° < 0$), hydrogen bonds and van der Waals interactions emerge as the dominant forces. Conversely, if both $\Delta S°$ and $\Delta H°$ are positive ($\Delta S° > 0$ and $\Delta H° > 0$), hydrophobic interactions take precedence in the interaction process. Electrostatic interactions are deemed the primary force when $\Delta S°$ is positive and $\Delta H°$ is negative ($\Delta S° > 0$ and $\Delta H° < 0$).[34] These thermodynamic parameters ($\Delta H°$ and $\Delta S°$) along with the Gibbs free energy ($\Delta G°$) are determined using van't Hoff eqs 3 and 4

$$\ln K_b = -\frac{\Delta H°}{RT} + \frac{\Delta S°}{R} \quad (3)$$

$$\Delta G° = \Delta H° - T\Delta S° \quad (4)$$

The thermodynamic parameters, $\Delta H°$ and $\Delta S°$, can be derived from a graphical representation of the natural logarithm of the equilibrium constant ($\ln K_b$) plotted against the reciprocal of the absolute temperature ($1/T$) at various

https://doi.org/10.1021/acsomega.4c00487
ACS Omega 2024, 9, 27071−27084

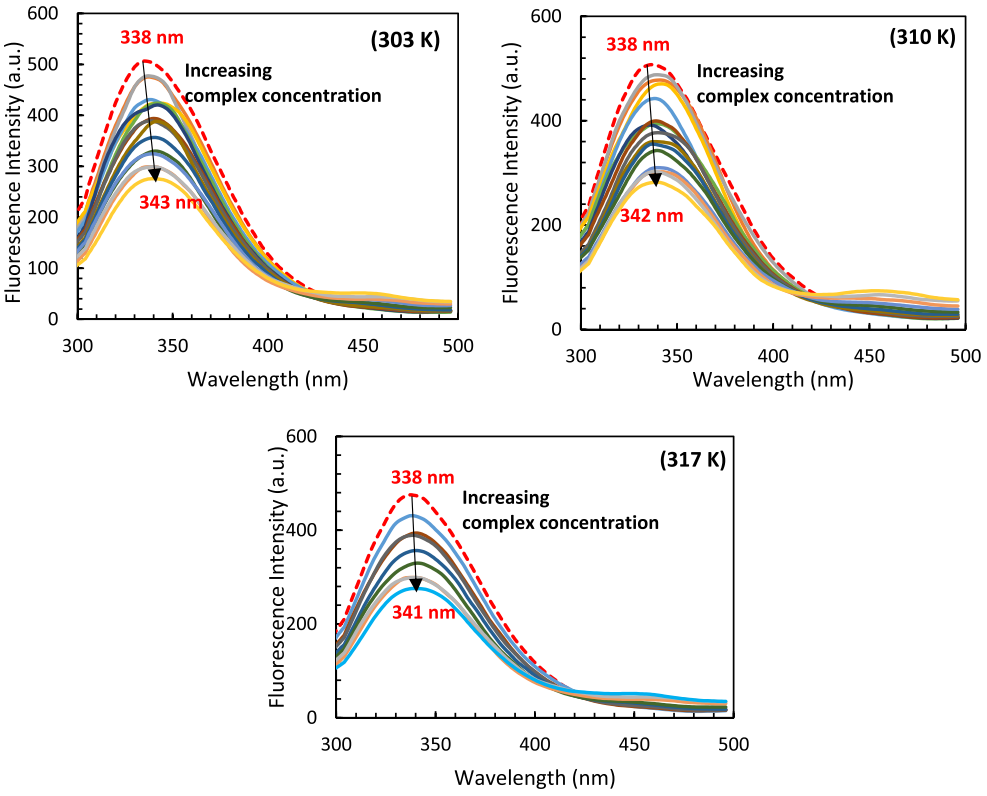

Figure 6. Fluorescence of BLC (dashed line) after interaction with Bi complex (solid lines) at 303, 310, and 317 K. [Bi complex] = 0−8.0 × 10^{-5} M.

temperature points. This graphical approach, depicted in Figure 7C, allows for the determination of these crucial thermodynamic quantities through the analysis of the line's slope and y-intercept. The calculated values of $\Delta H°$ and $\Delta S°$, obtained through this graphical analysis, are listed in Table 1.

The thermodynamic analysis of the interaction between the Bi complex and the BLC reveals several key insights. Notably, the $\Delta G°$ spectra exhibit negative values, indicating that the interaction process is spontaneous and favored from a thermodynamic perspective. Furthermore, both the $\Delta H°$ and $\Delta S°$ associated with this interaction are negative. This observation supports the hypothesis that van der Waals interactions and hydrogen bonding play crucial roles in facilitating formation of the BLC−Bi complex.

Structural Changes of Catalase. *Synchronous Fluorescence Assessment.* Two amino acids, Trp and Tyr, which are mainly responsible for the fluorescence emission of proteins, are sensitive to changes in the polarity of their microenvironment. Synchronous fluorescence spectroscopy is considered a useful technique for evaluating the polarity of the microenvironment of these two amino acids. In this technique, determination of the wavelength interval between the excitation and emission wavelengths ($\Delta\lambda$) is required. Here, SF spectra were recorded with $\Delta\lambda$ set at 15 and 60 nm for evaluating Tyr and Trp residues, respectively (Figure 8A,B). In this spectroscopic method, the shift in the location of the maximum wavelength indicates the polarity change of the Trp and Tyr microenvironment. As the Bi complex was added to the BLC solution, the position of the λ_{max} shifted to a limited extent toward longer wavelengths for both amino acids (from 285 to 287 nm for Tyr and from 280 to 285 nm for Trp). Based on this, it can be said that the interaction of the Bi complex with the BLC has led to a change in the microenvironment polarity of both amino acids. By comparing the amount of shift in the maximum wavelength for Trp and Tyr, it can be concluded that the binding site of the Bi complex to the enzyme is closer to the Trp than Tyr, so that Trp is more susceptible to microenvironmental polarity changes.[35]

Three-Dimensional Fluorescence Assessment. Three-dimensional fluorescence (3DF) is a useful technique in the analysis of protein structural changes induced by the interaction with small molecules. This technique shows the fluorescence emission intensity with different excitation and emission wavelengths. The 3DF spectrum of free BLC and BLC-Bi complexes is shown in Figure 9. Figure 9I corresponds to the 3DF spectrum of BLC, and as can be seen, four peaks are visible in it. A and B, which are assigned to the first and second order Rayleigh scattering, show reduced intensity in the presence of the Bi complex Peak 1 is attributed to the presence of three specific amino acids: tyrosine (Tyr), tryptophan (Trp), and phenylalanine (Phe). On the other hand, Peak 2 is associated with changes in the fluorescence behavior of the polypeptide backbone itself.[36] Upon interaction of BLC with the Bi complex, a notable change in the fluorescence characteristics is observed. Specifically, the intensities of both Peak 1 and Peak 2 decrease, indicating a quenching effect. Additionally, the maximum wavelength of these peaks undergoes a shift toward longer wavelengths, a phenomenon known as a red shift. These spectroscopic observations provide evidence for the unfolding of the polypeptide chain during the interaction between the BLC and the Bi complex.

Fourier Transform Infrared Assessment. Additional support for understanding the interaction between drugs and proteins is obtained through the findings of infrared spectros-

https://doi.org/10.1021/acsomega.4c00487
ACS Omega 2024, 9, 27071−27084

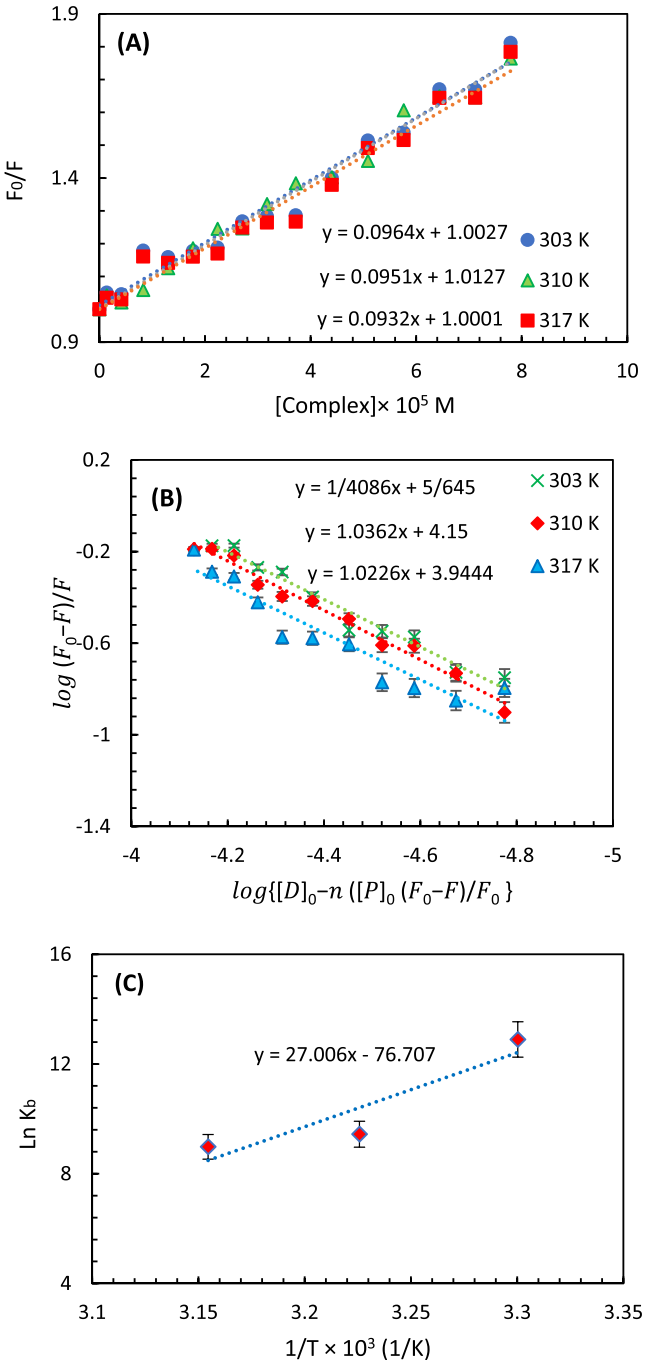

Figure 7. (A) Stern−Volmer plots of BLC after interaction with Bi complex at 303, 310, and 317 K. (B) The plot of log (F_0-F/F) is vs $\log\left\{[D]_0 - n\frac{[P]_0(F_0-F)}{F_0}\right\}$. (C) Arrhenius plots.

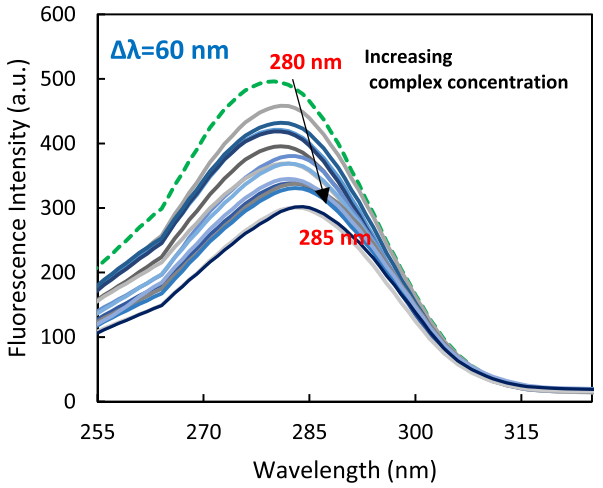

Figure 8. SF spectra of BLC (5×10^{-6} M) before (dash line) and after interaction with complex (solid lines). [Complex] = 0−7.52 × 10^{-5} M.

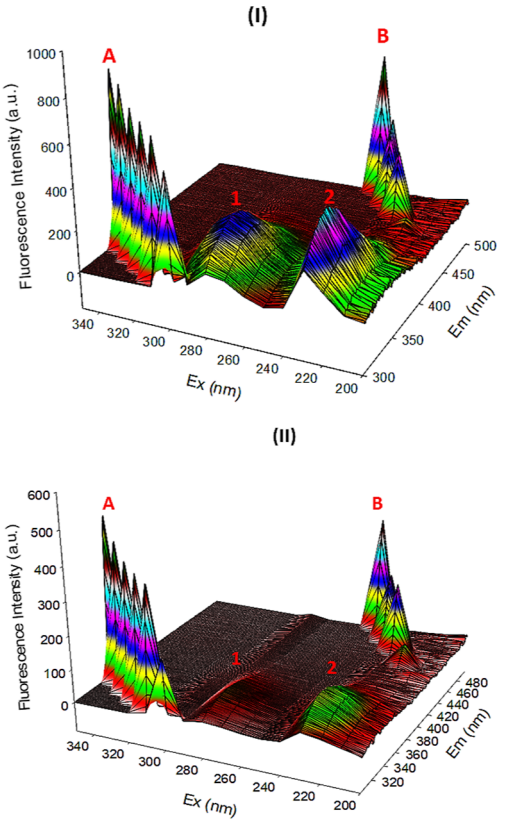

Figure 9. 3DF spectra of (I) BLC and (II) BLC−Bi complex.

copy. In the context of drug−protein complexation, observing changes or shifts in the IR spectrum within this range (1700−1500 cm^{-1}) can indicate the formation of a complex between the drug and the protein. Figure 10A shows the Fourier transform infrared (FT-IR) spectra of free BLC and BLC in the presence of the Bi complex. As depicted in the figure, the FT-IR spectrum of free BLC differs from that of the BLC−Bi complex. The distinct regions are highlighted by circles. The

Table 1. Interaction Parameters in the BLC−Bi Complex System

T (K)	n	K_{sv} ($\times 10^4$ M^{-1})	k_q ($\times 10^{12}$ M^{-1} s^{-1})	K_b ($M^{-1} \times 10^5$)	$\Delta G°$ (kJ mol^{-1})	$\Delta H°$ (kJ mol^{-1})	$\Delta S°$ (kJ mol^{-1} K^{-1})
303	1.11	0.96 ± 0.03	0.96 ± 0.03	3.97 ± 0.09	−31.40	−225.23	−0.63
310	1.02	0.95 ± 0.03	0.95 ± 0.03	0.12 ± 0.01	−26.29		
317	1.03	0.93 ± 0.02	0.93 ± 0.02	0.09 ± 0.003	−22.45		

https://doi.org/10.1021/acsomega.4c00487
ACS Omega 2024, 9, 27071−27084

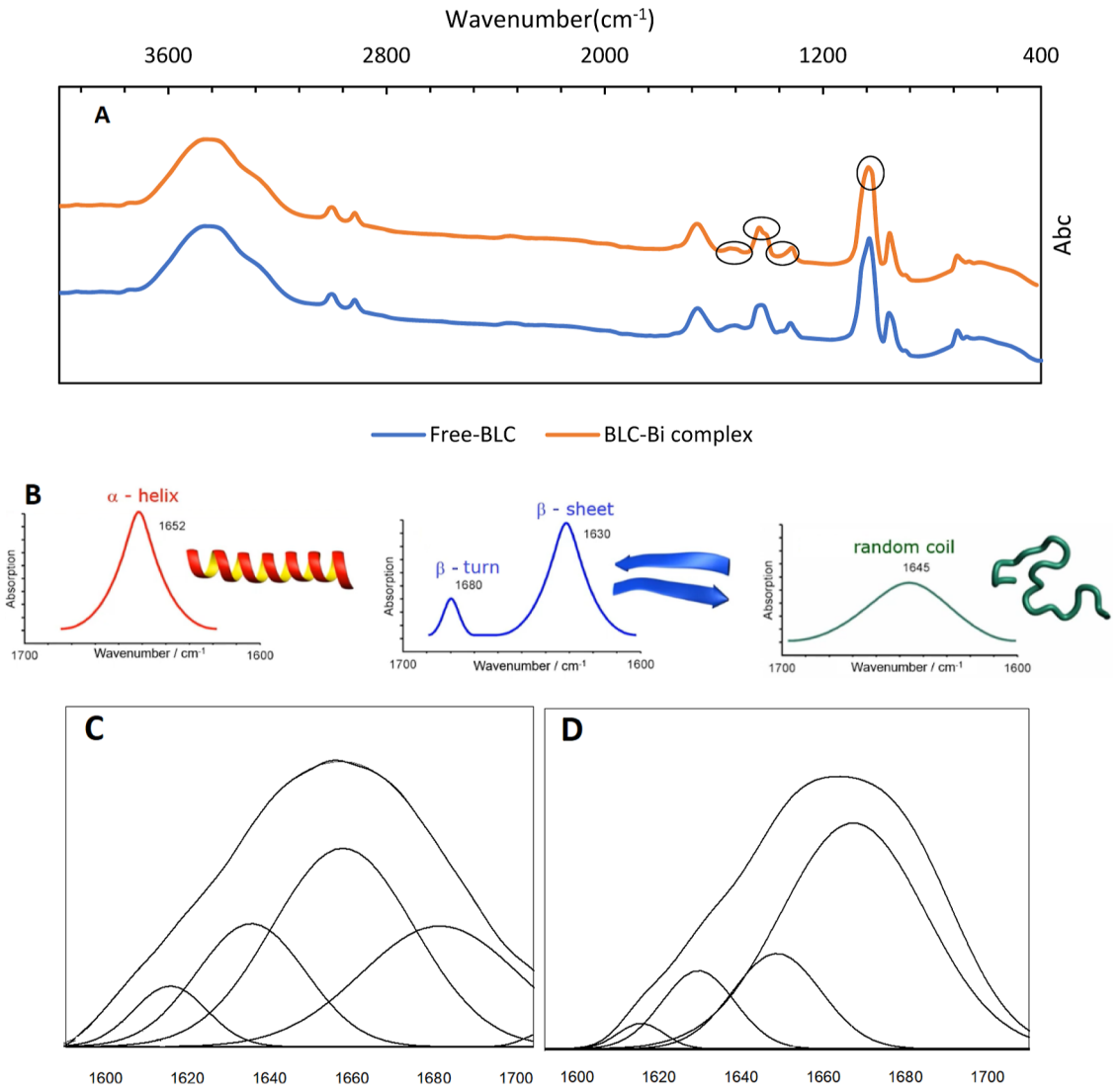

Figure 10. Changes in the FT-IR spectrum of BLC in the presence of the Bi complex (A), the peak locations of the amide I (1700−1600 cm^{-1}) bands for α-helix, β-sheet, β-turn, and random coil (B). Second-derivative resolution enhancement and curve-fitted amide I region for (C) free BLC and (D) BLC−Bi complex ([BLC]: = 5 × 10^{-6} M, Bi complex: = 5 × 10^{-6} M).

amide I band, ranging from 1600 to 1700 cm^{-1}, indicates various vibrations of the peptide moiety and has a relationship with the secondary structure of BLC. The peak locations of the amide I bands for α-helix, β-sheet, β-turn, and random coil are displayed in Figure 10B.[37,38] Using Fourier self-deconvolution provides a quantitative estimation of the area associated with each component representing a specific type of secondary structure. The FT-IR spectra were smoothed using a Savitzky−Golay filter, corrected for a constant baseline, and subjected to second-derivative analysis or Fourier deconvolution.[39,40] The effects on the secondary structure are more apparent in the deconvoluted spectra of catalase both in its free form (Figure 10C) and when complexed with Bi (Figure 10D). The free protein comprised 22% α-helix, 25% β-sheet, 25% β-turn, and 29% random coil structure. The predicted distribution of various secondary structures in the native catalase aligns with previously reported findings in the literature.[41,42] Upon the interaction of the Bicomplex with catalase, the α helix content experienced a decrease from 22 to 20.8%. The beta-sheet content showed a reduction from 25 to 24%. The beta-turn structure witnessed an increase from 25 to 29.2%. Meanwhile, the random coil decreased from 29 to 26% (Table 2). Hence, the binding process results in the observation of unfolding and diminished helical stability, which leads to alterations in the secondary structure of the proteins.[43]

Table 2. Secondary Structure Content of BLC for Two Systems—Free BLC and the BLC−Bi Complex

	protein secondary structures (%)			
system	α-helix	β-sheet	β-turn	random coil
free BLC	22	25	25	29
BLC−Bi complex	20.8	24	29.2	26

UV−Vis Assessment. Absorption of UV−vis light by proteins occurs mainly due to the presence of Trp, Tyr, and phenylalanine (Phe) residues with absorbance maxima at 280 nm. The UV−vis spectrum of catalase, which is a heme protein, also shows another peak in the region of 408 nm, which is related to the heme prosthetic group in this enzyme (Figure 11).[44] In this experiment, the absorption spectra of protein (5.0 × 10^{-6} M) upon titrating with the Bi complex (0−

https://doi.org/10.1021/acsomega.4c00487
ACS Omega 2024, 9, 27071−27084

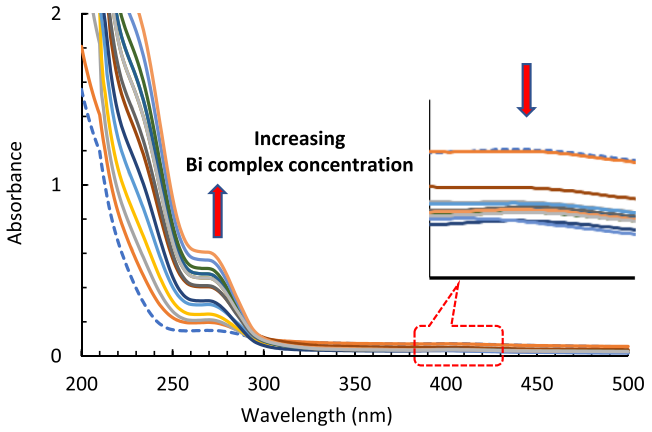

Figure 11. UV−vis spectra: Free BLC (dashed line) (5×10^{-6} M) and BLC−Bi complex (solid lines). [Bi complex] = 0−8.0×10^{-5} M.

8.0×10^{-5} M) were recorded from 200 to 500 nm. To eliminate the effect of the free Bi complex absorption on the UV spectra (the UV−vis spectrum of the free Bi complex is in the Supporting Information, Figure S1), a double beam UV−vis spectrophotometer was used and the corresponding Bi complex solution was taken as a reference solution in the measuring process.[32]

The absorption intensity of BLC at 280 nm increases in the presence of the Bi complex (hyperchromic change), confirming the binding of the Bi complex to the polypeptide chain. Additionally, the intensity of the peak related to the heme prosthetic group has also changed to some extent, indicating a slight structural disorder in the active site of the enzyme during the interaction.[7]

Transition Midpoint ($L_{1/2}$). UV−vis spectroscopic titrations provide a powerful tool for investigating ligand−protein interactions and monitoring the associated conformational changes in proteins. Figure 12 presents the results of such an

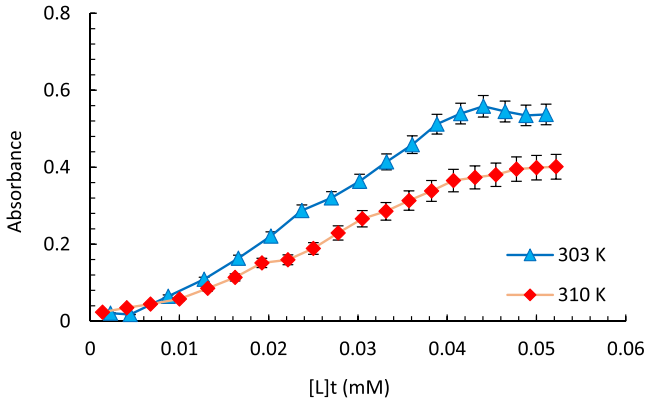

Figure 12. Absorbance changes of BLC at λ_{max} = 280 nm due to increasing the concentration of Bi complex at 300 and 310 K. [BLC] = 1×10^{-6} M, [Bi complex] = 0−0.52×10^{-4} M.

analysis, depicting the profiles of structural alterations undergone by the native form of BLC upon interaction with the Bi complex at two different temperatures. These structural changes have occurred in such a way that the absorbing groups of proteins are more exposed to UV−vis light, and with increasing concentration of Bi complex, the absorption peak intensity increases. Thus, the native and interacted forms of protein have different conformations, and transition between these two conformations is discussed under the above title.[45,46] $L_{1/2}$ is the ligand concentration required to induce 50% conformational change in the native protein. The $L_{1/2}$ values at two temperatures of 303 and 310 K were obtained as 0.025 and 0.0031 mM, respectively. The decrease of $L_{1/2}$ values at higher temperature confirms that the interaction process is exothermic.[47] These results are in agreement with the thermodynamic parameters previously determined for the system under study.

Examining the Safety of Bi Complex on Embryonic Mouse Fibroblast Cells. Cisplatin, as a well-known metal-based drug, has good effects on cancer cells, but due to numerous side effects and drug resistance, its use is limited. One of the important reasons for the side effects of cisplatin is the lack of differentiation between cancer and normal cells,[48] and for this reason, many efforts are made to synthesize metal complexes with lower risks. Therefore, we decided to check the safety of the Bi complex on mouse embryonic fibroblast NIH3T3 cells and compare its effects with cisplatin. As shown in Figure 13, the Bi complex only in one (highest) concentration causes a decrease in the number of cells below 50% compared to the control, while cisplatin shows negative effects in all concentrations. The IC_{50} comparison of two compounds (760 μM for Bi complex vs 56 μM for cisplatin) shows a better view of the safety of Bi complex on normal cells and makes us more hopeful for the creation of a safe metal complex.

Molecular Docking Analysis. To precisely identify the inhibition mechanism, molecular docking simulations were employed to predict the number of hydrogen bonds, interacting residues, and the specific binding sites of the Bi complex on BLC. During the docking process of the Bi complex with BLC, the nine conformations generated by Smina were evaluated and ranked according to the affinity scores presented in Table 3. The highest affinity observed for binding of the complex to BLC was determined to be −40.6 kJ mol^{-1}. Therefore, the docking results suggest that the Bi complex could bind to the enzymatic catalytic center, with energy values ranging from −40.6 to −34.7 for nine poses, which is close to the experimental ΔG° (−31.4 kJ mol^{-1}) mentioned earlier. The docking outcomes revealed the positioning of the Bi complex within the structural pockets of the catalase. It was found to be stabilized through hydrogen bonding and van der Waals interactions with the enzyme's residues.

Figure 14A illustrates that the Bi complex exhibits an affinity for binding to the alpha-helices and loops of the second domain on BLC. Figure 14B depicts the two-dimensional representation of the optimal conformer of the Bi complex binding to BLC. As illustrated in this figure, the complex forms three hydrogen bonds with ALA122, THR124, and ARG126 of BLC.

Additionally, numerous van der Waals interactions were observed with residues VAL125, ILE204, ALA249, and ALA253. These results and the observed interactions were consistent with the outcomes of the fluorescence studies. To conduct further investigations, the interaction energies between the Bi complex and amino acid residues within the active site of BLC are individually presented in Table 4.

CONCLUSIONS

Enzymes and proteins represent crucial drug targets, and drug−target interaction analysis is a key factor in drug

https://doi.org/10.1021/acsomega.4c00487
ACS Omega 2024, 9, 27071−27084

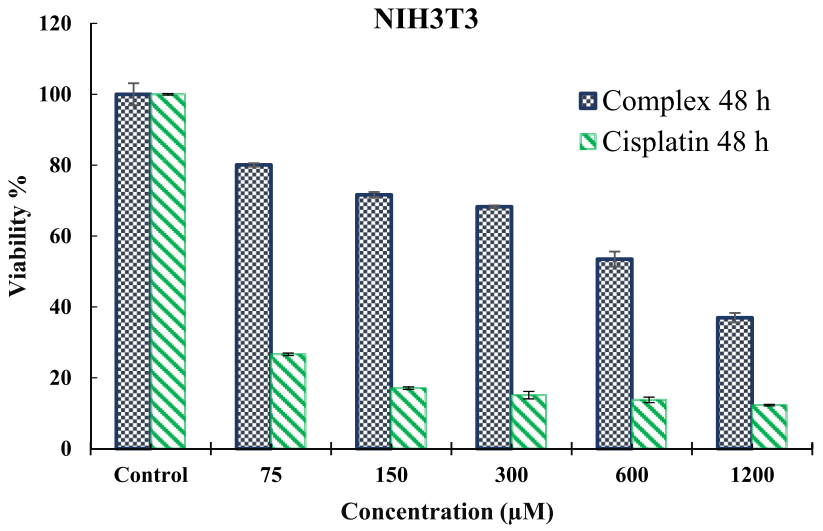

Figure 13. Assessing the safety of Bi complex on mouse embryonic fibroblast NIH3T3 cells and comparing with cisplatin The Bi complex does not significantly damage the cells. Instead, cisplatin at all concentrations causes the destruction of the cells.

Table 3. Smina Score of BLC with Different Conformers of Bi-Complex

pose	affinity of BLC (kJ mol^{-1})
1	−40.6
2	−40.2
3	−38.1
4	−37.2
5	−37.2
6	−36.4
7	−36.4
8	−36.0
9	−34.7

discovery.[44] While transition metals have been extensively studied in investigating the medicinal properties of metal complexes, main group elements have received comparatively less attention. In this research, a binuclear bismuth(III) complex was selected, and some of its biological abilities were evaluated. The Bi complex showed a high capacity to inhibit DPPH free radical, and its antioxidant activity was higher than those of many transition metals complexes. The Bi complex interacted with BLC through van der Waals forces and hydrogen bonds and quenched the fluorescence emission of the enzyme by a static mechanism. Its interaction with BLC led to the enhancement of the enzyme catalytic performance during the H_2O_2 decomposition. The results showed that the structure of the protein has changed to some extent during the interaction, and probably this change has led to the improvement of the catalytic activity of the enzyme. Furthermore, a comparative analysis of the effects of the Bi complex and cisplatin on mouse embryonic fibroblast NIH3T3 cells indicated that the synthesized complex is significantly safer than cisplatin. This finding underscores the potential

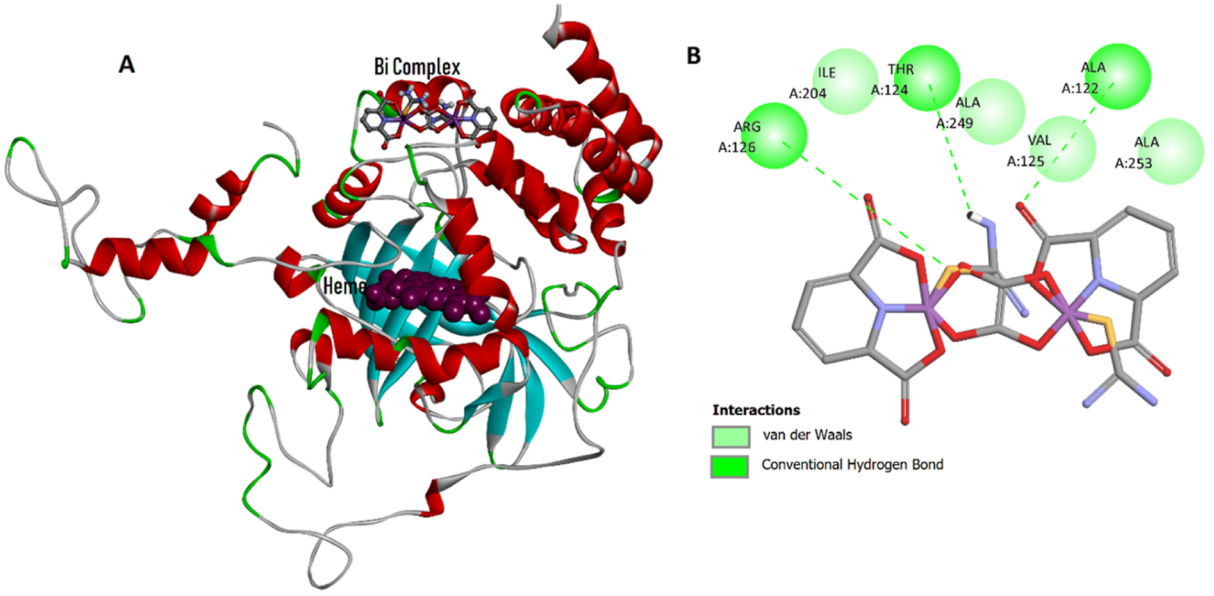

Figure 14. (A) Schematic illustration of the Bi complex binding sites on BLC. (B) Two-dimensional representation the docking results of Bi complex with BLC.

https://doi.org/10.1021/acsomega.4c00487
ACS Omega 2024, 9, 27071−27084

Table 4. Interaction Energy between the Bi-Complex and Responsive Amino Acid Residues of BLC in Molecular Docking

amino acid residues	interaction energy (kJ mol^{-1})
Arg126	−17.2659
Ala253	−11.1831
Val125	−10.5123
Ala122	−8.79324
Val246	−8.09126
Ala250	−5.74763
Asn461	−5.30077
Phe199	−5.12024
His465	−4.96312
Ser121	−4.29652
Ala249	−3.35125
His254	−2.62823
Thr124	−2.23321
Ile204	−1.55958

therapeutic value of the Bi complex, highlighting its safety profile in comparison to that of a widely used chemotherapeutic agent.

EXPERIMENTAL SECTION

Bismuth complex was synthesized under hydrothermal condition according to the method presented in ref 2 as follow: an aqueous solution (10 mL) of Bi $(NO_3)_3{\cdot}5H_2O$ (0.97 g, 2 mmol) was added to an aqueous solution (10 mL) of oxalic acid dihydrate (0.252 g, 2 mmol) and thiourea (0.152 g, 2 mmol) under stirring for 10 min. The resulting mixture was sealed in a 50 mL Teflon-lined autoclave and heated at 160 °C for 3 days. After this time, the solution was cooled to room temperature, filtered, and allowed to stand at room temperature. By slow solvent evaporation, the crystals of the Bi complex were obtained at 56% yield (based on Bi). The chemicals used in the synthesis and interaction processes were commercially obtained and used without further purification. Catalase from bovine liver (BLC) was procured from Sigma-Aldrich (USA). Stock solutions of the complex were prepared with a concentration of 5×10^{-3} M in deionized (DI) water. The BLC was dissolved in Tris−HCl buffer, and its concentration was determined using ultraviolet−visible (UV−vis) spectroscopy. The concentration of hydrogen peroxide was also measured by UV−vis spectroscopy, employing the molar extinction coefficient ε_{240} = 43.6 M^{-1} cm^{-1}, as reported in the literature.[19]

UV−vis absorption spectra were recorded by using a JASCO UV/vis-7850 double-beam spectrophotometer equipped with quartz cells having a path length of 1.0 cm. Fluorescence emission spectra were recorded in the range of 300−500 nm for a constant concentration of BLC (5.0×10^{-6} M). The complex solution (5×10^{-3} M stock solution) was gradually added to the BLC solution in a quartz cuvette by using an Agilent Cary Eclipse Fluorescence Spectrophotometer. To account for the effects of dilution, the fluorescence spectra intensity was corrected before data analysis. Additionally, inner filter effect corrections were performed to obtain accurate fluorescence intensity values.[49] Synchronous fluorescence spectra were recorded using delta wavelengths of 60 nm (in the range 250−310 nm) and 15 nm (in the range 260−320 nm). In this experiment, a fixed concentration of catalase (5.0×10^{-6} M) was titrated in the presence of different concentrations of the Bi complex (0−7.52×10^{-5} M) at room temperature.

FT-IR spectroscopy was employed to analyze the structural features of the BLC. The measurements were conducted using a JASCO-460 plus FT-IR spectrometer with the samples prepared as KBr disks. The spectral range investigated was 4000−400 cm-1, which encompasses the characteristic vibrational modes of various functional groups and secondary structure elements in proteins. To obtain the FT-IR spectrum of the free protein (BLC), the absorption spectrum of the Tris−HCl buffer solution was subtracted from the spectrum of the protein solution. This subtraction was performed at pH 7.40 and under room temperature conditions. The buffer subtraction step is crucial to eliminate the contribution of the solvent and to isolate the infrared absorption features specific to the protein. In order to obtained the changing of protein's secondary structure in the presence of Bicomplex, deconvolution (band curve-fitting)[38] of FT-IR spectra was done on OriginPro 10.1.0.178 software (https://www.originlab.com/origin).

Hirshfeld Surface Analysis. Intermolecular interactions for the Bi complex have been computed with the Crystal Explorer Ver. 3.1 program package[50] using Hirshfeld surface analysis[51] and 2D fingerprint plots.[52] Also, the percentage contributions for various intermolecular interactions for this complex have been computed. Hirshfeld surfaces are mapped using the normalized contact distance (d_{norm}) and is a ratio enclosing the distances of the nearest atom inside and outside to any surface point and the van der Waals radii of the atoms. d_i is the distance from a point on the surface to the nearest nucleus internal to the surface. d_e is distance from a point on the surface to the nearest nucleus external to the surface, and is a unique characteristic for each molecule.[51,53] $d_{norm} = (d_i - r_i^{vdw})/r_i^{vdw} + (d_e - r_e^{vdw})/r_e^{vdw}$; where r_i^{vdw} and r_e^{vdw} are the van der Waals radii of the atoms. Hirshfeld surface analysis and 2D fingerprinting offer valuable insights into both qualitative and quantitative aspects of intermolecular contacts, including distinctions between short and long interactions and the strength of these contacts, as indicated by colors and their intensities. The presence of white areas on the Hirshfeld surface signifies that intermolecular distances closely match the sum of the respective van der Waals radii. The red color indicates the shorter intermolecular interactions, and the blue color shows the distances longer than the sum of the respective van der Waals radii.

Antioxidant Capacity Investigation. The antioxidant potential of the Bi complex can be assessed by using the DPPH• free radical. This radical exhibits absorption at λ_{max} = 517 nm, facilitating easy monitoring of changes in its concentration. In this experiment, if the Schiff base compound interacts with the free radical in a manner that inhibits its activity, the solution's color will shift from yellow to purple, accompanied by a decrease in absorption intensity. The study investigates two variables: time (30 and 60 min) and concentration. The changes in DPPH• absorption (at constant concentration) in the presence of the ligand and complexes (ranging from 0.25 to 125 mg L^{-1}) are recorded. The antioxidant capacity of the complexes for inhibiting •DPPH is calculated using eq 5[54]

$$\text{scavenging activities (\%)} = A_0 - \frac{A}{A_0} \times 100 \quad (5)$$

A_0: control absorbance. A: sample absorbance.

https://doi.org/10.1021/acsomega.4c00487
ACS Omega 2024, 9, 27071−27084

BLC Performance Investigation. BLC has the function of breaking down hydrogen peroxide into water and oxygen. The level of BLC activity can be readily monitored because hydrogen peroxide, the substrate, has absorption at a wavelength of 240 nm, allowing for the easy tracking of changes in its concentration. During the experiment, the concentration of the enzyme (1.0×10^{-8} M) and its substrate (55.5×10^{-3} M) remains constant, while the concentration of **C1−C3** varies ($0-1.7 \times 10^{-7}$ M). The inhibition of BLC activity by **C1−C3** is calculated using eq 6[55]

$$i\ \% = \frac{\Delta A_1}{\Delta A_0} \times 100 \tag{6}$$

ΔA_1: sample absorbance changes. ΔA_0: control absorbance changes. i = degree of inhibition.

Interaction Mechanism Investigation. In the development of new reagents with biological capabilities, studying their interactions with important biological molecules is crucial. In this research, the interaction between the Bi complex and catalase was investigated in a buffer medium (0.1 M Tris, pH = 7.4) containing 0.1 M NaCl. Fluorescence quenching studies were conducted at different temperatures (303, 310, and 317 K), while UV−vis titration was performed at 303 K. The complex stock solution (5×10^{-3} M) was prepared using deionized water. The catalase solution, with a concentration of 1×10^{-4} M, was prepared by using Tris buffer and stored in a refrigerator at 4 °C until testing. The concentration of the catalase solution was determined by measuring the absorbance intensity at a wavelength of 280 nm.

Examining the Safety of Bi Complex on Embryonic Mouse Fibroblast Cells. The MTT method was used to measure the cell viability and safety of the Bi complex on mouse embryonic fibroblast NIH3T3 cells in comparison with the known drug cisplatin. For this purpose, the cells were cultured according to standard protocols[56] for 3 weeks to be exposed to five different concentrations of the complex and cisplatin. Five concentrations included 75, 150, 300, 600, and 1200 μM of the Bi complex and cisplatin [n = 3, ±SD (standard deviation)], which were separately exposed to the cells for 48 h. The protocol of staining cells by MTT was carried out in detail, and the absorbance of formazan crystals dissolved in dimethyl sulfoxide was read by ELISA Reader at a wavelength of 570 nm.

Molecular Docking Study. Smina software was employed to illustrate the mode of interaction between the Bi complex and BLC. Smina is a version of AutoDock Vina with a specific emphasis on enhancing scoring and minimizing energy.[57] The Bi complex structure, identified by the CIF extension file with the code CCDC-2079968, was retrieved from the Cambridge Crystallographic Data Center (http://www.ccdc.cam.ac.uk/). Subsequently, Open Babel software was employed to convert the CIF file of the Bi complex into a.mol2 extension file.[58] The BLC crystal structure was acquired from the RCSB Protein Data Bank with the PDB code 1TGU (https://www.rcsb.org/). As all four chains of BLC exhibit similarity, we opted for chain A in conducting theoretical studies. The purification process involved eliminating heteroatoms and solvent molecules from the structure. Subsequently, polar hydrogens and Kollman charges were added into BLC. A grid box measuring 28 × 22 × 26 Å was centered on the Bi complex, positioned at coordinates 40.25, 34.80, and 23.79 in the X, Y, and Z planes, with a grid spacing of 1 Å. Then, the Lamarckian genetic algorithm was employed to search for binding sites on the target. Furthermore, Molegro Molecular Viewer 2.5 was utilized to compute the interaction energy between the optimal pose of the docked complex and the catalase binding site, assessing each amino acid individually (http://www.molegro.com/mmv-product.php).

■ ASSOCIATED CONTENT

Supporting Information

The Supporting Information is available free of charge at https://pubs.acs.org/doi/10.1021/acsomega.4c00487.

CIF and CHECKCIF files of the Bi complex (CIF)

UV−vis spectrum of the Bi complex (PDF)

■ AUTHOR INFORMATION

Corresponding Author

Fereshteh Shiri − *Department of Chemistry, University of Zabol, Zabol 9861335856, Iran*; orcid.org/0000-0003-2879-9347; Phone: +98 5431232186; Email: fereshteh.shiri@gmail.com, Fereshteh.shiri@uoz.ac.ir; Fax: +98 5431232186

Authors

Zahral Alimoradi − *Department of Chemistry, University of Zabol, Zabol 9861335856, Iran*

Somaye Shahraki − *Department of Chemistry, University of Zabol, Zabol 9861335856, Iran*

Zohreh Razmara − *Department of Chemistry, University of Zabol, Zabol 9861335856, Iran*

Mostafa Heidari-Majd − *Department of Medicinal Chemistry, Faculty of Pharmacy, Zabol University of Medical Sciences, Zabol 9861615881, Iran*

Complete contact information is available at: https://pubs.acs.org/10.1021/acsomega.4c00487

Author Contributions

Z.A.: performed experiments and investigations; F.S.: initiated the research, led the project team, conducted the computational study, and contributed to writing, reviewing, and editing the manuscript; S.S.: assisted in resolving experimental technical issues, conducted data analysis, and contributed to manuscript writing; Z.R.: synthesized the Bi complex and contributed to writing the manuscript; and M.H.-M.: conducted the MTT method and contributed to writing the manuscript.

Funding

This work was funded by the University of Zabol [Grant code: IR-UOZ-GR-0144].

Notes

The authors declare no competing financial interest.

■ ACKNOWLEDGMENTS

The authors thank Zabol University for all support provided.

■ REFERENCES

(1) Yang, Y.; Ouyang, R.; Xu, L.; Guo, N.; Li, W.; Feng, K.; Ouyang, L.; Yang, Z.; Zhou, S.; Miao, Y. Review: Bismuth complexes: synthesis and applications in biomedicine. *J. Coord. Chem.* **2015**, *68*, 379−397.

(2) Razmara, Z.; Eigner, V.; Dusek, M. Single crystal structure features of a new Bi (III) complex, for preparation an effective bleaching catalyst. *Polyhedron* **2022**, *216*, 115725.

(3) Orellana-Tavra, C.; Köppen, M.; Li, A.; Stock, N.; Fairen-Jimenez, D. Biocompatible, crystalline, and amorphous bismuth-based metal−organic frameworks for drug delivery. *ACS Appl. Mater. Interfaces* **2020**, *12*, 5633−5641.
(4) Rosário, J. d. S.; Moreira, F. H.; Rosa, L. H. F.; Guerra, W.; Silva-Caldeira, P. P. Biological activities of bismuth compounds: An overview of the new findings and the old challenges not yet overcome. *Molecules* **2023**, *28*, 5921.
(5) Yang, H.; Zhao, Y.; Guo, Y.; Wu, B.; Ying, Y.; Sofer, Z.; Wang, S. Surfactant-Mediated Crystalline Structure Evolution Enabling the Ultrafast Green Synthesis of Bismuth-MOF in Aqueous Condition. *Small* **2024**, *20*, 2307484.
(6) Shahraki, S.; Samareh Delarami, H.; Saeidifar, M. Catalase inhibition by two Schiff base derivatives, Kinetics, thermodynamic and molecular docking studies. *J. Mol. Liq.* **2019**, *287*, 111003.
(7) Dehghan, G.; Rashtbari, S.; Dastmalchi, S.; Iranshahi, M. Noncompetitive inhibition of bovine liver catalase by lawsone: kinetics, binding mechanism and in silico modeling approaches. *Iran. J. Pharm. Res.* **2020**, *19*, 383.
(8) Shahraki, S.; Samareh Delarami, H.; Poorsargol, M.; Sori Nezami, Z. Structural and functional changes of catalase through interaction with Erlotinib hydrochloride. Use of Chou's 5-steps rule to study mechanisms. *Spectrochim. Acta, Part A* **2021**, *260*, 119940.
(9) Shahraki, S.; Delarami, H. S.; Saeidifar, M.; Nejat, R. Catalytic activity and structural changes of catalase in the presence of Levothyroxine and Isoxsuprine hydrochloride. *Int. J. Biol. Macromol.* **2020**, *152*, 126−136.
(10) Rashtbari, S.; Dehghan, G.; Yekta, R.; Jouyban, A. Investigation of the binding mechanism and inhibition of bovine liver catalase by quercetin: Multi-spectroscopic and computational study. *Bioimpacts: Bi* **2017**, *7*, 147−153.
(11) Samal, R. R.; Mishra, M.; Subudhi, U. Differential interaction of cerium chloride with bovine liver catalase: A computational and biophysical study. *Chemosphere* **2020**, *239*, 124769.
(12) Xu, M.; Cui, Z.; Zhao, L.; Hu, S.; Zong, W.; Liu, R. Characterizing the binding interactions of PFOA and PFOS with catalase at the molecular level. *Chemosphere* **2018**, *203*, 360−367.
(13) Shahraki, S.; Saeidifar, M.; Delarami, H. S.; Kazemzadeh, H. Molecular docking and inhibitory effects of a novel cytotoxic agent with bovine liver catalase. *J. Mol. Struct.* **2020**, *1205*, 127590.
(14) Ghobadi, R.; Divsalar, A.; Harifi-Mood, A. R.; Saboury, A. A.; Eslami-Moghadam, M. How a promising anti-cancer derivative of palladium consisting phen-imidazole ligand affects bovine liver catalase functionality. *J. Photochem. Photobiol., A* **2018**, *364*, 288−296.
(15) Glorieux, C.; Calderon, P. B. Catalase, a remarkable enzyme: targeting the oldest antioxidant enzyme to find a new cancer treatment approach. *Biol. Chem.* **2017**, *398*, 1095−1108.
(16) Galasso, M.; Gambino, S.; Romanelli, M. G.; Donadelli, M.; Scupoli, M. T. Browsing the oldest antioxidant enzyme: catalase and its multiple regulation in cancer. *Free Radical Biol. Med.* **2021**, *172*, 264−272.
(17) Pieniążek, A.; Czepas, J.; Piasecka-Zelga, J.; Gwoździński, K.; Koceva-Chyła, A. Oxidative stress induced in rat liver by anticancer drugs doxorubicin, paclitaxel and docetaxel. *Adv. Med. Sci.* **2013**, *58*, 104−111.
(18) Pal, S.; Dey, S. K.; Saha, C. Inhibition of catalase by tea catechins in free and cellular state: a biophysical approach. *PLoS One* **2014**, *9*, No. e102460.
(19) Khataee, S.; Dehghan, G.; Yekta, R.; Rashtbari, S.; Maleki, S.; Khataee, A. The protective effect of natural phenolic compound on the functional and structural responses of inhibited catalase by a common azo food dye. *Food Chem. Toxicol.* **2022**, *160*, 112801.
(20) Koohshekan, B.; Divsalar, A.; Saiedifar, M.; Saboury, A.; Ghalandari, B.; Gholamian, A.; Seyedarabi, A. Protective effects of aspirin on the function of bovine liver catalase: A spectroscopy and molecular docking study. *J. Mol. Liq.* **2016**, *218*, 8−15.
(21) Samal, R. R.; Kumari, K.; Sahoo, Y.; Mishra, S. K.; Subudhi, U. Interaction of artemisinin protects the activity of antioxidant enzyme catalase: A biophysical study. *Int. J. Biol. Macromol.* **2021**, *172*, 418−428.
(22) Shahraki, S.; Shiri, F.; Razmara, Z. Improving enzymatic performance of antioxidant enzyme catalase in combination with [Mn(phen)$_2$Cl.H$_2$O]Cl.tu complex. *Appl. Organomet. Chem.* **2023**, *37*, No. e7061.
(23) El-Lateef, H. M. A.; El-Dabea, T.; Khalaf, M. M.; Abu-Dief, A. M. Recent Overview of Potent Antioxidant Activity of Coordination Compounds. *Antioxidants* **2023**, *12*, 213.
(24) Nouri, H.; Mansouri-Torshizi, H.; Shahraki, S. Exploring the functional changes and binding mechanism of bovine liver catalase in the presence of Schiff base complexes, Comprehensive spectroscopic studies. *J. Iran. Chem. Soc.* **2021**, *18*, 3281−3294.
(25) Shahraki, S.; Majd, M. H.; Heydari, A. Novel tetradentate Schiff base zinc (II) complex as a potential antioxidant and cancer chemotherapeutic agent: Insights from the photophysical and computational approach. *J. Mol. Struct.* **2019**, *1177*, 536−544.
(26) Khan, S. N.; Islam, B.; Yennamalli, R.; Sultan, A.; Subbarao, N.; Khan, A. U. Interaction of mitoxantrone with human serum albumin: Spectroscopic and molecular modeling studies. *Eur. J. Pharm. Sci.* **2008**, *35*, 371−382.
(27) Wang, Q.; Huang, C.-r.; Jiang, M.; Zhu, Y.-y.; Wang, J.; Chen, J.; Shi, J.-h. Binding interaction of atorvastatin with bovine serum albumin: Spectroscopic methods and molecular docking. *Spectrochim. Acta, Part A* **2016**, *156*, 155−163.
(28) Zhang, Y.-F.; Zhou, K.-L.; Lou, Y.-Y.; Pan, D.-q.; Shi, J.-H. Investigation of the binding interaction between estazolam and bovine serum albumin: multi-spectroscopic methods and molecular docking technique. *J. Biomol. Struct. Dyn.* **2017**, *35*, 3605−3614.
(29) Wang, B.-L.; Pan, D.-Q.; Zhou, K.-L.; Lou, Y.-Y.; Shi, J.-H. Multi-spectroscopic approaches and molecular simulation research of the intermolecular interaction between the angiotensin-converting enzyme inhibitor (ACE inhibitor) benazepril and bovine serum albumin (BSA). *Spectrochim. Acta, Part A* **2019**, *212*, 15−24.
(30) Jameson, D. M. *Introduction to fluorescence*; Taylor & Francis, 2014; .
(31) Zhang, J.; Chen, L.; Zhu, Y.; Zhang, Y. Study on the molecular interactions of hydroxylated polycyclic aromatic hydrocarbons with catalase using multi-spectral methods combined with molecular docking. *Food Chem.* **2020**, *309*, 125743.
(32) Kou, S.-B.; Lin, Z.-Y.; Wang, B.-L.; Shi, J.-H.; Liu, Y.-X. Evaluation of the binding behavior of olmutinib (HM61713) with model transport protein: Insights from spectroscopic and molecular docking studies. *J. Mol. Struct.* **2021**, *1224*, 129024.
(33) Shahraki, S.; Samareh Delarami, H.; Mansouri-Torshizi, H.; Nouri, H. Investigation of kinetics and thermodynamics in the interaction process between two pyridine derived Schiff base complexes and catalase. *J. Mol. Liq.* **2021**, *334*, 116527.
(34) Ross, P. D.; Subramanian, S. Thermodynamics of protein association reactions: forces contributing to stability. *Biochemistry* **1981**, *20*, 3096−3102.
(35) Ambika, S.; Sundrarajan, M. Green biosynthesis of ZnO nanoparticles using Vitex negundo L, extract: Spectroscopic investigation of interaction between ZnO nanoparticles and human serum albumin. *J. Photochem. Photobiol., B* **2015**, *149*, 143−148.
(36) Huo, M.; Zhao, L.; Wang, T.; Zong, W.; Liu, R. Binding mechanism of maltol with catalase investigated by spectroscopy, molecular docking, and enzyme activity assay. *J. Mol. Recognit.* **2020**, *33*, No. e2822.
(37) Krimm, S.; Bandekar, J. Vibrational spectroscopy and conformation of peptides, polypeptides, and proteins. *Adv. Protein Chem.* **1986**, *38*, 181−364.
(38) Byler, D. M.; Susi, H. Examination of the secondary structure of proteins by deconvolved FTIR spectra. *Biopolymers* **1986**, *25*, 469−487.
(39) Arora, T.; Verma, R.; Kumar, R.; Chauhan, R.; Kumar, B.; Sharma, V. Chemometrics based ATR-FTIR spectroscopy method for rapid and non-destructive discrimination between eyeliner and mascara traces. *Microchem. J.* **2021**, *164*, 106080.

https://doi.org/10.1021/acsomega.4c00487
ACS Omega 2024, 9, 27071−27084

(40) Gładysz, M.; Król, M.; Kościelniak, P. Differentiation of red lipsticks using the attenuated total reflection technique supported by two chemometric methods. *Forensic Sci. Int.* **2017**, *280*, 130−138.
(41) Xu, M.; Sheng, Z.; Lu, W.; Dai, T.; Hou, C. Probing the interaction of mutiwalled carbon nanotubes and catalase: mutispectroscopic approach. *J. Biochem. Mol. Toxicol.* **2012**, *26*, 493−498.
(42) Hu, Y.; Da, L. Insights into the selective binding and toxic mechanism of microcystin to catalase. *Spectrochim. Acta, Part A* **2014**, *121*, 230−237.
(43) Charbonneau, D.; Beauregard, M.; Tajmir-Riahi, H.-A. Structural analysis of human serum albumin complexes with cationic lipids. *J. Phys. Chem. B* **2009**, *113*, 1777−1784.
(44) Chi, Z.; Liu, R.; Zhang, H. Potential enzyme toxicity of oxytetracycline to catalase. *Sci. Total Environ.* **2010**, *408*, 5399−5404.
(45) Eslami Moghadam, M.; Saidifar, M.; Divsalar, A.; Mansouri-Torshizi, H.; Saboury, A. A.; Farhangian, H.; Ghadamgahi, M. Rich spectroscopic and molecular dynamic studies on the interaction of cytotoxic Pt (II) and Pd (II) complexes of glycine derivatives with calf thymus DNA. *J. Biomol. Struct. Dyn.* **2016**, *34*, 206−222.
(46) Shahraki, S.; Shiri, F.; Mansouri-Torshizi, H.; Shahraki, J. Characterization of the interaction between a platinum (II) complex and human serum albumin: spectroscopic analysis and molecular docking. *J. Iran. Chem. Soc.* **2016**, *13*, 723−731.
(47) Heydari, A.; Mansouri-Torshizi, H. Design, synthesis, characterization, cytotoxicity, molecular docking and analysis of binding interactions of novel acetylacetonatopalladium (II) alanine and valine complexes with CT-DNA and BSA. *RSC Adv.* **2016**, *6*, 96121−96137.
(48) Xu, F.; Zhang, L.; Heidari Majd, M.; Shiri, F.; Karimi, P.; Guo, X. Increase delivery, cytotoxicity, stability and induction of apoptosis in cisplatin by establishing a new complex with methotrexate. *J. Drug Delivery Sci. Technol.* **2023**, *86*, 104683.
(49) Lakowicz, J. R. *Principles of fluorescence spectroscopy*; Springer Science & Business Media, 2013; .
(50) Wolff, S.; Grimwood, D.; McKinnon, J.; Turner, M.; Jayatilaka, D.; Spackman, M. *Crystal explorer*; University of Western Australia Crawley: Australia, 2012; .
(51) McKinnon, J. J.; Jayatilaka, D.; Spackman, M. A. Towards quantitative analysis of intermolecular interactions with Hirshfeld surfaces. *Chem. Commun.* **2007**, *37*, 3814−3816.
(52) Spackman, M. A.; McKinnon, J. J. Fingerprinting intermolecular interactions in molecular crystals. *CrystEngComm* **2002**, *4*, 378−392.
(53) McKinnon, J. J.; Mitchell, A. S.; Spackman, M. A. Hirshfeld surfaces: a new tool for visualising and exploring molecular crystals. *Chem.—Eur. J.* **1998**, *4*, 2136−2141.
(54) Shahraki, S.; Razmara, Z.; Shiri, F. A paramagnetic oxalato-bridged binuclear copper (II) complex as an effective catalase inhibitor, Spectroscopic and molecular docking studies. *J. Mol. Struct.* **2020**, *1208*, 127865.
(55) Chen, L.; Zhang, J.; Zhu, Y.; Zhang, Y. Interaction of chromium (III) or chromium (VI) with catalase and its effect on the structure and function of catalase: an in vitro study. *Food Chem.* **2018**, *244*, 378−385.
(56) Sargazi, A.; Barani, A.; Heidari Majd, M. Synthesis and apoptotic efficacy of biosynthesized silver nanoparticles using acacia luciana flower extract in MCF-7 breast cancer cells: Activation of bak1 and bclx for cancer therapy. *BioNanoScience* **2020**, *10*, 683−689.
(57) Koes, D. R.; Baumgartner, M. P.; Camacho, C. J. Lessons learned in empirical scoring with smina from the CSAR 2011 benchmarking exercise. *J. Chem. Inf. Model.* **2013**, *53*, 1893−1904.
(58) O'Boyle, N. M.; Banck, M.; James, C. A.; Morley, C.; Vandermeersch, T.; Hutchison, G. R. Open Babel: An open chemical toolbox. *J. Cheminf.* **2011**, *3*, 33.

https://doi.org/10.1021/acsomega.4c00487
ACS Omega 2024, 9, 27071−27084